ADVANCED ENERGY & SUSTAINABILITY RESEARCH
www.advenergysustres.com

Printable Carbon-Based Thermogalvanic Cells

Pedro Santos Candiotto de Oliveira, Ujwala Ail, Zia Ullah Khan, Reverant Crispin, and Dan Zhao**

Thermogalvanic cells (TGCs) can convert low-grade heat directly into electricity through reversible redox reactions induced by temperature gradient. As a unique member of the thermoelectric device family, TGCs provide advantages such as cost-effective and sustainable materials, a relatively high Seebeck coefficient, and the ability to generate continuous output power. To date, the challenge toward commercializing TGCs lies in developing functional electrode materials that can be produced on a large scale. Herein, the performance of printable activated carbon (AC) as the electrode in TGC is investigated. The multilayer printing of the AC electrodes provides increasing capacitance and improves the maximum output power of the TGC. This is mainly due to the decrease in the device's total resistance thanks to the large surface area of thick AC electrodes. The advanced understanding of the interface between the printed electrode and electrolyte paves the road toward printable and sustainable TGC.

1. Introduction

Against the backdrop of a deepening energy crisis, there has been a growing array of technologies emerging with the goal to convert renewable energy into electricity. Low-grade heat from industrial plants, geothermal sources, and solar radiation forms one of the most attractive energy sources because of their large amount, but also the most challenging one because of the low energy density.[1] Thermoelectric materials could directly convert heat into electricity via the ability of coupling heat and current flow.

Three distinct categories of thermoelectric devices have been created to accommodate various material characteristics. The most well-known thermoelectric generators (TEGs) composed of doped semiconductors or semimetals generate a continuous output power with constant input heat. Yet only a restricted range of materials, primarily BiTe-based alloys, demonstrate functionality in TEGs for harvesting low-grade heat. The use of tellurium increases the material cost while the high-temperature processes for their synthesis lead to a negative impact of CO_2 emission. On the contrary, ionic thermoelectric materials are mostly electrolytes with sustainable composition that can be processed via low-cost and low-temperature methods. The generated ionic thermal voltage can be orders of magnitude higher than from TEGs, and output power is extracted by charging supercapacitors. However, the ionic thermoelectric charged supercapacitors can only continuously generate output power via charging and discharging under intermittent heating, which unavoidably reduces their efficiency.[2]

The third category, electrolytes with reversible redox couple combine the characteristics of the other two counterparts. Thermogalvanic cells (TGCs) constructed with such electrolytes can generate a constant current under a temperature difference (ΔT) via charge transfer between the electrolyte and electrodes. Compared with typical materials used in TEGs (Bi_2Te_3), the TGCs could utilize aqueous-based solutions that are far ecofriendlier and more cost-effective.[3] The maximum output power of TGCs depends on the Seebeck coefficient α (defined as the ratio between thermal voltage and applied ΔT), applied ΔT, and the internal resistance of the device ($P_{max} = (\alpha \Delta T)^2/4R_{in}$).

Numerous research has been successfully conducted to enhance the Seebeck coefficient and reduce the internal resistance of TGC. Material tailoring technologies have been proved effective to improve the Seebeck coefficient of the redox electrolytes from 1.4 mV K^{-1} up to 4 mV K^{-1}.[4–7] The internal resistance of a TGC is dependent on the ion and mass transport in the electrolyte, the electronic transport through the electrode and the electrical contacts, and the charge diffusion and transfer in the electrodes.[8–10] High concentration of redox couples (normally above 1 M) are typically chosen in TGCs to increase the output power by increasing the redox current.[11,12] For the electrode, the classic candidate is platinum in TGCs due to its air stability without insulating oxide surface.[13–15] To decrease the material and fabrication cost of TGCs, organic and carbon-based materials that are rather stable in air have been applied as electrodes in TGCs. Wijeratne et al. reported that the performance of spin-coated conducting polymer PEDOT: TOS in TGC could be competitive to Pt electrodes with increasing thickness to 2 μm.[16] The use of carbon nanostructure with a large surface area has been a common strategy to decrease the charge transfer

P. S. Candiotto de Oliveira, U. Ail, Z. Ullah Khan, R. Crispin, D. Zhao
Laboratory of Organic Electronics
Department of Science and Technology
Linköping University
SE-60174 Norrköping, Sweden
E-mail: reverant.crispin@liu.se; dan.zhao@liu.se

The ORCID identification number(s) for the author(s) of this article can be found under https://doi.org/10.1002/aesr.202400428.

© 2025 The Author(s). Advanced Energy and Sustainability Research published by Wiley-VCH GmbH. This is an open access article under the terms of the Creative Commons Attribution License, which permits use, distribution and reproduction in any medium, provided the original work is properly cited.

DOI: 10.1002/aesr.202400428

resistance between the electrode surface and the redox electrolyte in TGCs. Carbon nanotubes,[17,18] Pt-decorated carbon nanotubes (CNTs) aerogel,[19] carbon cloth /paper,[20] porous carbon,[21] and carbon nanowire[22] have been successfully applied as the TGC electrodes.

Despite the promising performance in the demonstrated TGCs, it is challenging to realize scalable low-cost manufacturing using those electrodes.[6,23–26] In this work, we explored activated carbon (AC) that is commonly used in supercapacitors[10,27] as the air-stable and high surface area electrode materials in the TGCs. The electrochemical and thermoelectric performance of AC as the electrode for TGCs were systematically investigated. We discovered that increasing thickness of the AC electrodes by multiple printing could efficiently decrease the internal resistance of the TGCs while maintaining the same Seebeck coefficient. The output power doubled for five layers printed AC electrodes compared to single layer and was close to the one of bare platinum electrodes. Understanding the electrochemical and thermoelectric processes at the interface between AC electrodes and redox electrolytes (such as potassium ferro/ferricyanide commonly used in TGCs) will advance the development of TGC materials. This knowledge will facilitate the creation of scalable, cost-effective thermogalvanic devices tailored for practical applications.

2. Results and Discussion

Initially, the AC ink was stencil printed on substrate (graphite foil or glass) and dried for 1 h at 100 °C for different characterizations. The thickness of AC electrodes increases from 100 to 500 µm almost linearly when printing from 1 to 5 layers (Figure S1a, Supporting Information). The conductivity of the dried AC layers (printed over glass) of the different thicknesses is between 0.5 and 0.7 S cm^{-1} (Figure S1b, Supporting Information), which agrees with previous reports.[28] The scanning electron microscopy (SEM) images of the printed AC of 1 and 5 layers (Figure S1c,d, Supporting Information) show similar porous surface and confirm that there is no obvious difference in morphology between them. It is important to note that the AC ink used here can be printed via screen-printing technology (Figure S2, Supporting Information).

Cyclic voltammetry (CV) was used to characterize the electrochemical properties of the printed AC electrodes. 0–5 layers of printed AC on graphite foil were used as the working electrodes (WEs). The electroactive solutions are composed of the redox-active species (10 mM $K_4[Fe(CN)_6]$ and 10 mM $K_3[Fe(CN)_6]$) and 1.0 M KCl. Note that KCl 1.0 M was added as supporting electrolyte to suppress migration effects.[29,30] When using non-redox-active KCl electrolyte (**Figure 1**a), the cells show capacitive response with increasing current for thicker electrodes. As comparison, cyclic voltammograms in the same electrolytes were also measured for platinum WE. Pt electrode has shown the lowest current when compared to AC, due to its relatively small capacitance. With the addition of the redox couple, peaks around 0.25 V in addition to the capacitive current can be observed (Figure 1b), due to the formal potential where the redox interconversion of the $[Fe(CN)_6]^{3-/4-}$ occurs.[16,31] The electrochemical window selected for all the CV measurements was between −0.1 and +0.6 V to avoid side reactions and degradation beyond these potentials. Well-defined peaks could be observed for all electrodes.

The ratio and the separation between the anodic and cathodic peaks in a CV curve are typically used to assess the reversibility of an electrochemical redox reaction.[29] The calculated peak ratio for all the AC thicknesses in Figure 1b is between 0.92 and 0.95, indicating relatively good reversibility, as the ideal ratio is 1.00. The peak-to-peak separation should be smaller than 57 mV for highly reversible one-electron redox reactions.[29,32] The peak separation Pt electrodes is 83 mV (Figure S3, Supporting Information), showing quasi-reversible electron transfer process. The separation for AC samples increases to the range of 90–140 mV (increases with thickness, Figure S3, Supporting Information), which still indicates quasi-reversible electron transfer process.[29,33] The electrochemical irreversibility is due to the slower electron transfer at the electrode compared to mass transport, which here is related with the increase in thickness of the AC electrodes.[29] Despite the better reversibility on platinum electrodes, the performance of AC electrodes is comparable at low concentration of redox molecules and they have substantially higher capacitive performance, as indicated by the box-like behavior of the CV curves in Figure 1a. From Figure 1c, and S4, Supporting Information, the comparison with platinum electrodes confirms that all the

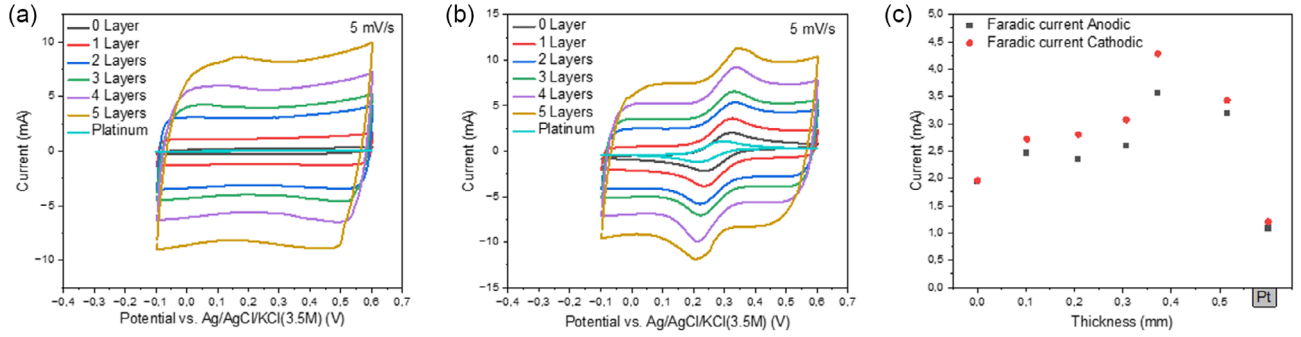

Figure 1. CV characterization of the AC electrodes of increasing thickness and Pt electrode for comparison in a) 1 M KCl and b) 20 mM $[Fe(CN)_6]^{3-/4-}$ and 1.0 M KCl electrolyte. c) Faradic current obtained from AC electrodes with different thicknesses and Pt electrode. The voltammograms were obtained at a scan rate of 5 mV s^{-1}.

© 2025 The Author(s). Advanced Energy and Sustainability Research published by Wiley-VCH GmbH

26999412, 0, Downloaded from https://advanced.onlinelibrary.wiley.com/doi/10.1002/aesr.202400428 by Linkoping Universitet, Wiley Online Library on [20/05/2025]. See the Terms and Conditions (https://onlinelibrary.wiley.com/terms-and-conditions) on Wiley Online Library for rules of use; OA articles are governed by the applicable Creative Commons License

current from the platinum systems is due to the faradaic process of the electron transfer between the redox molecules dissolved in the electrolyte.

The increase in the surface area of the AC electrodes extends the diffusion path of the electrolyte ions in the electrode for the formation of the double layer.[29,34] CV measurements and galvanostatic charge and discharge of the AC electrodes (Figure S4, Supporting Information) confirm the increasing capacitance for thicker AC electrodes. Hence, the capacitive current (i_C) and total peak current (i_p) increase with the thickness of the AC electrodes (Figure S5, Supporting Information). The anodic and cathodic Faradic currents of all the electrodes were extracted from Figure 1a,b and plot in Figure 1c. Pt electrodes show the lowest Faradic current likely due to the smaller surface area compared to AC and graphite electrodes. However, the Faradic current for AC electrodes only increases slightly with the thickness. This is an indication that the electron transfer with the $[Fe(CN)_6]^{3-/4-}$ ions occurs mostly on the surface of the electrode, different from the ions which forms the double layer inside the electrode. The reason could be that the negatively charged AC (due to the presence of carboxylate ions on its surface) repels the negatively charged $[Fe(CN)_6]^{3-/4-}$ ions. Similar phenomenon was previously observed in PEDOT electrodes.[16] Moreover, the mass transport of the $[Fe(CN)_6]^{3-/4-}$ ions from the electrolyte into the electrode could be slowed down by the tortuosity of the paths. Nevertheless, these results still confirm that the AC electrode is suitable for the reversible redox reaction of $[Fe(CN)_6]^{3-}/[Fe(CN)_6]^{4-}$.

Considering that the high concentration of redox couple could provide large output current in TGCs, we investigated the effect of electrolyte concentration. CV measurements using AC electrode of two layers (≈200 µm thickness) were tested with increasing concentrations of $[Fe(CN)_6]^{3-/4-}$ (20, 100, 200, and 400 mM in 1.0 M KCl). As shown in **Figure 2**a, increasing concentration of redox species greatly enhances the peak current, which relates to electron transfer and output current in the TGCs. At the same time, the peak separation of the anodic and cathodic peaks (Figure S6, Supporting Information) increases with the concentration of redox species, indicating that the diffusion of the ionic species in the electrolytes is hindered. This is due to mass

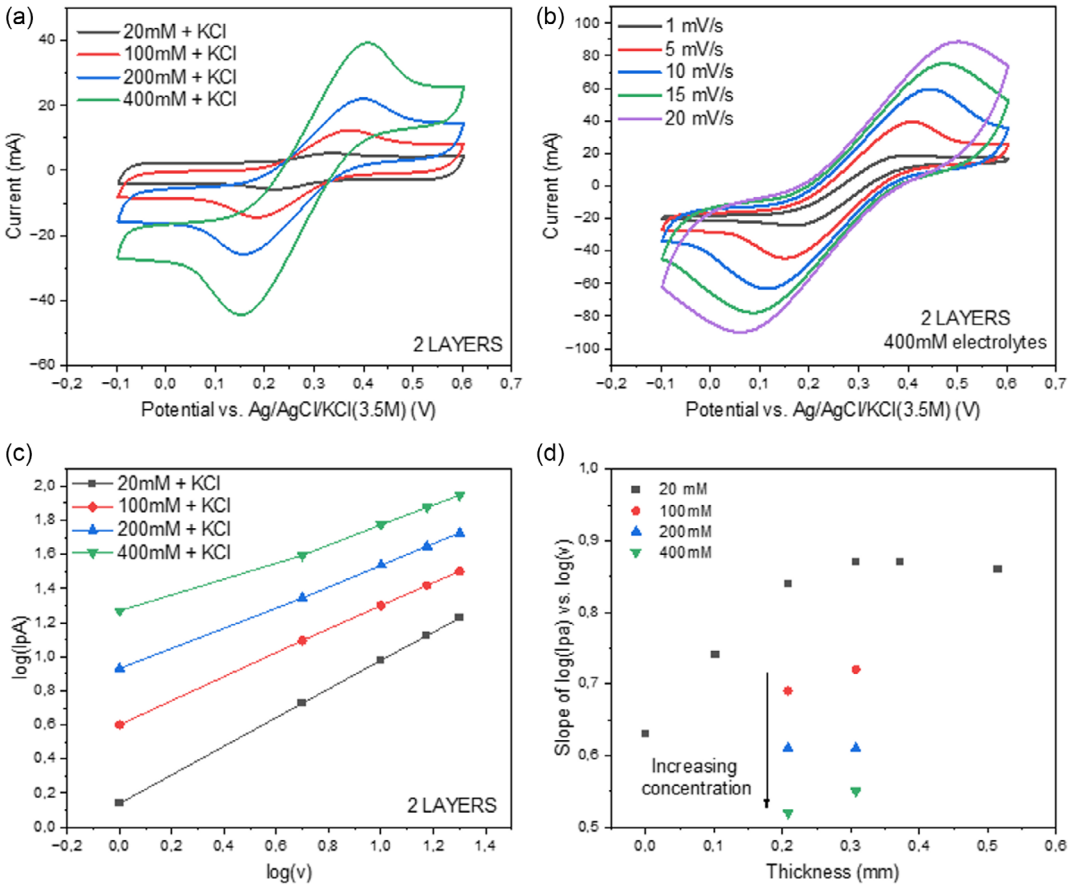

Figure 2. a) Cyclic voltammograms of two-layer AC in different concentrations of $[Fe(CN)_6]^{3-/4-}$, ranging from 20 to 400 mM (with KCl of 1.0 M). b) Cyclic voltammograms of two-layer AC in 400 mM $[Fe(CN)_6]^{3-/4-}$ (with KCl of 1.0 M) at different scan rates (from 1 to 20 mV s^{-1}). c) Slope of the logarithm of peak current versus the logarithm of the scanning rate square root for two layers AC electrode with different concentrations of $[Fe(CN)_6]^{3-/4-}$. d) Slope of the logarithm of peak current versus the logarithm of the scanning rate square root for AC with different thickness at fixed electrolyte concentration of 20 mM, and with different concentrations of the redox species in the electrolytes for the fixed thicknesses of 200 µm (two layers) and 300 µm (three layers).

© 2025 The Author(s). Advanced Energy and Sustainability Research published by Wiley-VCH GmbH

26999412, 0, Downloaded from https://advanced.onlinelibrary.wiley.com/doi/10.1002/aesr.202400428 by Linkoping Universitet, Wiley Online Library on [20/05/2025]. See the Terms and Conditions (https://onlinelibrary.wiley.com/terms-and-conditions) on Wiley Online Library for rules of use; OA articles are governed by the applicable Creative Commons License

transport effects of diffusion and migration, as the migration is not fully limited by supporting electrolyte in the case of high-concentration analytes.[34]

The current originated from capacitive effect and redox reaction responds differently to the change of scan rate, as shown in the equations below, where the redox reaction based one is the so-called Randles–Sevcik equation:[29]

$$i_C = \mathrm{ACv} \quad (1)$$

$$i_p = 0.446n\mathrm{FAC}\left(\frac{n\mathrm{FDv}}{\mathrm{RT}}\right)^{1/2} \quad (2)$$

where n is the number of electrons involved in the redox reaction, A is the surface area of the electrode, D is the diffusion coefficient of the oxidized specie, C is the bulk concentration of the analyte, F is the Faraday constant, R is the molar gas constant, and T is the temperature.

To investigate the kinetic of the electron transfer between the redox couple and AC electrode, different scan rates were used. Figure 2b shows an example of the CV curves of the highest studied electrolyte concentration using different scan rates (the same set of CV curves of other electrolyte concentration is shown in Figure S7, Supporting Information). Applying a linearization to the plot of the logarithm of the peak current versus the logarithm of the scan rate for each concentration leads to slope value between 0.5 and 1.0 (Figure 2c). The extreme values of 0.5 and 1.0 correspond to diffusion-controlled and pseudo-capacitive controlled current response, respectively.[29,33] The slopes for AC electrodes of 1–5 layers with 20 mM $[Fe(CN)_6]^{3-/4-}$ were calculated from the CV curves exhibited in Figure S8, Supporting Information. The same study for different scan rates at 20 mM $[Fe(CN)_6]^{3-/4-}$ was performed for platinum electrodes, where the well-defined current peaks related to electron transfer between electrolyte redox species at the electrode interface are shown in Figure S9a, Supporting Information. From the anodic current peaks, the slope between $\log(I)$ versus $\log(\nu)$ was calculated as well in Figure S9b, Supporting Information, is equal to 0.61, hence a bit lower than pure graphite foil (Figure 2d), and demonstrating that in standard platinum electrodes, the process of electron transfer is limited mainly by diffusion. Further discussion about Randles–Sevcik relation can be found in Figure S11, Supporting Information.

As shown in Figure 2d (black squares), the slope values of all the electrodes thickness measured with diluted electrolyte fall between 0.60 and 0.88, showing mixed controlling process. The increasing slope value for AC below 250 μm indicates that the current is dominated more and more by the capacitive process with increasing AC thickness. This is due to the large contribution of the double layer at low redox couple concentration, which increases linearly with the thickness, while the faradaic process does not increase on the same proportion as the thickness and hence has a lower impact for AC thicker than 250 μm. The choice of two-layer AC electrodes for the CV analysis with different electrolytes concentrations was based on the results exposed in Figure 2d, where the two-layer thickness was the last one before the saturation of the slope in 0.88 for thicker layers.

For one fixed AC thickness (≈200 μm), the charge transfer kinetic shifts from pseudo-capacitive controlled to diffusion controlled with the increase in redox couple concentration, as the slope decreases from 0.84 to 0.52 (indicated by the arrow in Figure 2d). This is because the high concentration of redox couple enhances the contribution of the diffusion-limited Faradic current in the total current. This also indicates the penetration of the redox molecules to some extent in thicker electrode, as noticed for slightly increasing Faradic current with the electrodes thicknesses. It is interesting to notice that a transition in kinetic takes place for AC thickness between 200 and 300 μm in concentrated electrolyte (400 mM), where capacitive contribution saturated in diluted electrolytes and started to contribute to concentrated electrolytes (details in Figure S10, Supporting Information). The kinetic analysis implies that increasing thickness of AC electrodes could enhance the collected current in TGCs to a certain level.

The electric properties of AC electrodes of different thickness and Pt electrode were investigated with impedance spectroscopy and direct current (DC) resistance characterization in a TGC with two-electrode configuration. The same printing process was used to print different layers of AC on glass substrates with current collector (thermal evaporate Au rings, details can be found in Experiment Section). Note that the different substrates could lead to small variation in the thickness of the AC electrodes. Cell assembled with platinum electrodes on the same configuration was also characterized to be compared with the AC electrodes. Based on the features of the Nyquist plot in **Figure 3**a and previous work,[16] we proposed the equivalent circuit (inset in Figure 3a). The two capacitive elements are related to double layer and Faradaic capacitance.[16] R_s accounts for series resistance includes the electronic resistance in the electrode, ionic resistance in the electrolyte, and contact resistance at electrode/electrolyte interface; R_{ct} accounts for the charge transfer resistance; R_{bulk} is related to the ionic transport in the bulk of the electrode material; and Warburg component W represents the mass transport limitation phenomena at the low frequency in the impedance measurement. These three resistances values were simulated from the equivalent circuit utilizing the software RelaxIS.

As shown in Figure 3b, the simulated R_{ct} (blue triangles) decreases dramatically with increasing AC thickness and saturates for thicknesses above 200 μm. This is in consistency with the above discussion that the redox species could penetrate into AC layer to certain extent. The gradually decreasing trend of R_s (red circles) can be ascribed to the larger surface area and smaller resistance of the thicker AC layers. R_{bulk} (green triangles) decreases for thin AC electrodes and maintains constant for thicker ones. As the electrolyte is the same for all of the measurements, the decreasing trend in R_{bulk} could be explained by the increasing surface area together with the contribution from ionic tortuosity.[8,35–37] Interestingly, the performance of platinum electrodes was in the same range of the AC electrodes with higher thicknesses, showing the high performance of these easy assembled AC electrodes, comparable to the state-of-the-art platinum electrodes, well known in the literature of TGCs.[5,7]

The overall DC resistance (R_{DC}) of cells with different AC thickness and platinum electrodes was investigated by directly applying fixed potential and measuring the correspondent saturated current. As shown in Figure S12, Supporting information, a charging current peak appeared first when applying a DC

© 2025 The Author(s). Advanced Energy and Sustainability Research published by Wiley-VCH GmbH

26999412, 0, Downloaded from https://advanced.onlinelibrary.wiley.com/doi/10.1002/aesr.202400428 by Linkoping Universitet, Wiley Online Library on [20/05/2025]. See the Terms and Conditions (https://onlinelibrary.wiley.com/terms-and-conditions) on Wiley Online Library for rules of use; OA articles are governed by the applicable Creative Commons License

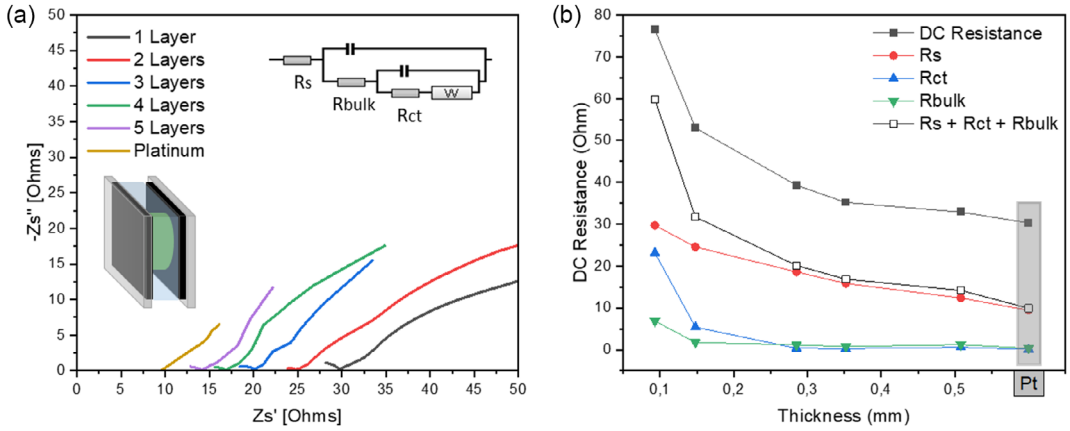

Figure 3. The electric characterization of the AC electrodes and platinum electrodes for comparison. a) Nyquist plot from impedance spectroscopy measurement for AC with different thickness and Pt electrodes. Inset shows the schema of the assembled device (left) and the equivalent circuits (right). b) Measured DC resistance and the different resistive contributions extracted from EIS spectra in Figure 3a.

potential to the cell, followed by a constant saturation current. The DC resistance can be calculated from the slope of potential versus current plot. The measured DC resistance (filled black squares) with increasing AC thickness is compared with the total resistances adding up from the simulated ones (open black squares). The calculated DC value is smaller than the measured one due to the difference between DC and AC measurement. Nevertheless, both curves show the tendency of sharp decrease for AC below 250 µm thickness and slowing down for the one above 250 µm. This is in agreement with the kinetic analysis in Figure 2d, where capacitive process started to contribute to concentrated electrolytes. The electric characterization of AC with different thickness shows that increasing the thickness could reduce the internal resistance of the TGCs. Once more, the platinum electrodes DC resistance matched that of the thicker AC electrodes, confirming the promising performance of the AC TGCs.

After evaluating the effect of AC thickness on the internal resistance of the TGCs, the impact on Seebeck coefficient was also investigated. As shown in **Figure 4**a, the Seebeck coefficient for devices with electrodes of different AC thickness and Pt shows reasonably similar values with the average of $-1.4\,\mathrm{mV\,K^{-1}}$, which is in good agreement with previous studies.[8,31,38] The output current and power generated from TGCs with different electrodes were measured with applied ΔT (8 K–10 K). As shown in Figure 4b, the normalized maximum output power increases with the thickness of the AC electrodes. This is mainly due to the decreasing internal resistance (as shown in Figure 3b) that results in higher current density for TGC with thicker AC electrodes. The normalized maximum power from Figure 4b is compared with calculated value ($P_{\max} = \alpha^2/4R_{\mathrm{DC}}$) in Figure 4c.[3,39,40] The calculated power increased with the electrode thickness and saturated at 0.35 µm due to the slow-down change in DC resistance. However, it is interesting to notice that the measured maximum power increases for the whole study range of AC electrodes thickness and for platinum. This is probably associated with the fact that the resistance of the device was measured at RT while the TGCs were operated at averagely higher temperature.

Finally, the performance of our TGC of low-cost printed AC electrodes was compared with previously reported TGCs over the years. **Table 1** summarizes the materials of electrode and electrolyte of the TGCs together with their Seebeck coefficient and normalized maximum power. For pure $[Fe(CN)_6]^{4-/3-}$ electrolytes,

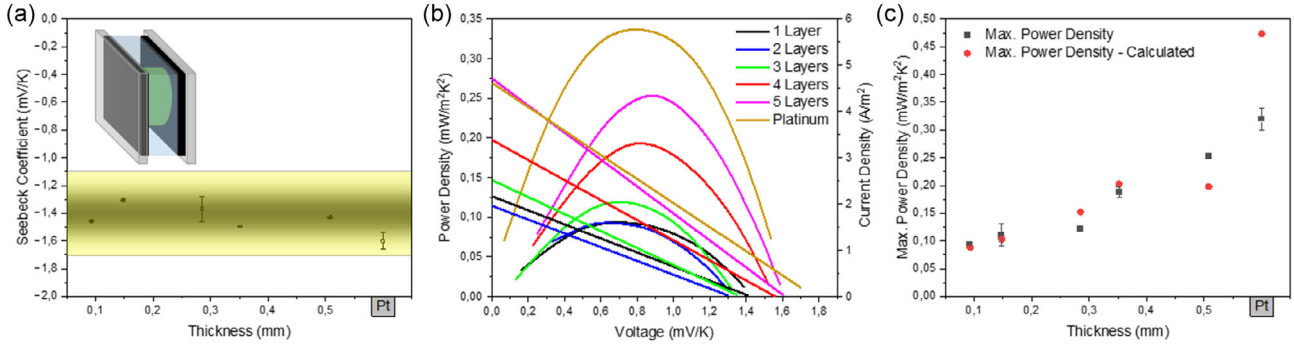

Figure 4. Thermogalvanic performance of the cells of with different AC thickness and platinum electrodes. a) Seebeck coefficient. b) Output current and power versus different output voltage (normalized with ΔT from 8 to 10 K). Raw data are shown in Figure S13, Supporting Information. c) Measured and calculated maximum output power of the TGCs with different AC thickness and platinum electrodes.

© 2025 The Author(s). Advanced Energy and Sustainability Research published by Wiley-VCH GmbH

26999412, 0, Downloaded from https://advanced.onlinelibrary.wiley.com/doi/10.1002/aesr.202400428 by Linkoping Universitet, Wiley Online Library on [20/05/2025]. See the Terms and Conditions (https://onlinelibrary.wiley.com/terms-and-conditions) on Wiley Online Library for rules of use; OA articles are governed by the applicable Creative Commons License

26999412, 0, Downloaded from https://advanced.onlinelibrary.wiley.com/doi/10.1002/aesr.202400428 by Linkoping Universitet, Wiley Online Library on [20/05/2025]. See the Terms and Conditions (https://onlinelibrary.wiley.com/terms-and-conditions) on Wiley Online Library for rules of use; OA articles are governed by the applicable Creative Commons License

Table 1. Comparison of TGCs properties with other works reported in the literature.

Electrode material	Electrolyte material	Seebeck [mV K^{-1}]	Normalized max. power [mW m^{-2} K^{-2}]	Printed	Reference
Platinum	$KI_3/KI + \alpha$-CD	2.00	0.01	No	[5]
Carbon fabric paper/graphite plates	$[Fe(CN)_6]^{4-/3-}$ + GdmCl	3.73	7.08	No	[27]
CNTs aerogel sheet	$[Fe(CN)_6]^{4-/3-}$	1.43	0.13	No	[19]
Porous carbon electrode	$[Fe(CN)_6]^{4-/3-}$	1.40	0.24	No	[21]
Multi walled CNTs Buckypaper	$[Fe(CN)_6]^{4-/3-}$	1.40	0.38	No	[18]
Platinum	$CA^{\cdot-}/CA^{2-}$ in AN + EtOH	2.60	0.51	No	[7]
N-CNW@CC	$[Fe(CN)_6]^{4-/3-}$ + GdmCl	3.70	8.56	No	[22]
N-CNW@CC	$[Fe(CN)_6]^{4-/3-}$	–	0.48	No	[22]
A-CC	$K_3[Fe(CN)_6]/(NH_4)_4[Fe(CN)_6]$	1.43	1.80	No	[20]
Single walled nanotubes-rGO	$[Fe(CN)_6]^{4-/3-}$	–	0.33	No	[17]
Au@Carbon paper	$[Fe(CN)_6]^{4-/3-}$ + GdmCl + FA	3.10	1.59	No	[41]
AC 5 Layers	$[Fe(CN)_6]^{4-/3-}$	1.43	0.25	Yes	This work
Pt foil	$[Fe(CN)_6]^{4-/3-}$	1.60	0.32	No	This work

the Seebeck coefficient was equal to 1.4 mV K^{-1}, as expected from the literature, showing again this property is intrinsic to the electrolyte.[18–21] The normalized maximum power output of our TGC ranks among the best when utilizing pure aqueous $[Fe(CN)_6]^{4-/3-}$ electrolytes, while employing low-cost, printable AC electrodes.[17–21] Improving the Seebeck coefficient of the electrolytes could substantially enhance the maximum power of the TGCs.[6,22] The effect of different molecules and additives was studied and reported, showing Seebeck coefficients of 3.7 mV K^{-1} for $[Fe(CN)_6]^{4-/3}$ with guanidinium chloride,[22] 2.0 mV K^{-1} for $KI_3/KI + \alpha$-CD[5] and 2.6 mV K^{-1} for $CA^{\cdot-}/CA^{2-}$ in AN + EtOH.[7] These electrolytes could be possibly utilized in TGC with printed AC electrodes, which has been demonstrated here with standard electrolyte. The modification of electrolytes has also been reported for i-TEs, where Wang et al. (2024) have reported gold and carbon paper electrodes with $[Fe(CN)_6]^{4-/3}$, guanidinium chloride and formamide, generating 3.10 mV K^{-1} the Seebeck and 1.59 mW m^{-2} K^{-2} power output.[41]

3. Conclusion

Printable AC was investigated as the electrodes of TGCs. We investigated the electrochemical properties of the printed AC electrode of different thicknesses. Combined with impedance and DC characterization, we discovered that increasing the thickness of AC reduces the internal resistance of the TGC by 50%. This was mainly due to the contribution from large interface between electrode and electrolyte, which improves the ionic transport in the bulk of the electrode material, charge transfer process, and the contact resistance. The improved electric property for thicker AC electrodes doubled the maximum output power of the TGC. The TGC with thick AC electrodes showed performance approaching platinum electrodes. Our study revealed the charge diffusion and transfer process between potassium ferro/ferricyanide and the AC electrode with complex porous structure and proved that AC is indeed promising to be used as the printable electrode for TGCs. Those findings pave the way for the development of large-scale and sustainable TGCs/modules with low-cost manufacture that will advance the field of thermal energy harvesting.

4. Experimental Section

Materials: The AC ink utilized for electrodes preparation was purchased from redox.me and used after homogenization. According to the manufacturer, the ink has a composition of 30–50% of water, 10–25% of AC, 1–3% of carbon black, as conductivity additive, and 0.2–0.8% of styrene-butadiene copolymer and 0.2–0.8% of carboxymethyl cellulose sodium salt as binder. Potassium hexacyanoferrate (II) trihydrate, potassium ferricyanide (III), and potassium chloride were purchased from Sigma Aldrich and utilized without further purification for the electrolytes preparation. PDMS Sylgard 184, utilized as an electrolyte container, was purchased from Dow Corning, and prepared in the 1:10 ratio. Graphite foil SIGRAFLEX was purchased from SGL carbon and utilized after cleaning with isopropanol.

Device Preparation: For electrolytes, different concentrations of ferrocyanide/ferricyanide ($[Fe(CN)_6]^{3-/4-}$, 20, 100, 200, 400 mM) were dissolved in water together with 1.0 M KCl. Pure 1.0 M KCl solution was also prepared for control measurements. For the electrodes, graphite foils were cut in the dimensions of 4 cm × 1 cm. AC ink was then stencil printed over the graphite foils in a limited area of 1 cm × 1 cm in different thicknesses, ranging from 100 to 500 µm. Each 100 µm corresponds to one printed layer, hence, the samples were labeled as AC 1–5 layers. The three-electrode cells were assembled by submerging the electrodes in a beaker filled with electrolyte.

The TGCs used in electric and thermoelectric characterization are prepared by assembling two electrodes on glass with a precut PDMS chamber. The glass slides were cleaned with soap, then rinsed with water, dried with nitrogen flow, rinsed with isopropanol, and finally dried in an oven. A thin layer of gold (180 nm) was evaporated on the glass slides with a mask shaped as a ring to work as the current collector, below the gold, 30 nm of chromium were evaporated to guarantee the adhesion. AC was again stencil printed over the gold ring in a round shape of 16 mm diameter in different thicknesses, ranging from 100 (1 layer) to 500 µm (5 layers). A 10 mm diameter hole was cut in a PDMS film (2 mm thickness). A pair of electrodes printed over glass slides patterned with gold was glued to each side of the PDMS film with uncured PDMS. The cell was then cured at 70 °C for 1 h to cure the PDMS glue and seal the device. The electrolyte

© 2025 The Author(s). Advanced Energy and Sustainability Research published by Wiley-VCH GmbH

was prepared by dissolving 0.4 M potassium ferrocyanide/ferricyanide in water (0.2 M of each salt). The electrolyte was injected into the cell with a syringe through an aperture made on the top of the PDMS film.

Characterization: The graphite foil printed with AC was the WE, a platinum gauze with larger area than WE acted as counter electrode (CE); while the reference electrode (RE) utilized was Ag/AgCl/KCl (3.5 M). The CV was scanned in the voltage range of −0.1 to +0.6 V, with the scan rates of 1, 5, 10, 15, and 20 mV s^{-1}, in a Bio-Logic SP 200 Potentiostat/Galvanostat. Galvanostatic charge–discharge tests were also performed in the current density of 2 mA cm^{-2} in the same voltage range as the CVs for the electrolytes containing 20 mM of potassium ferrocyanide/ferricyanide and the pure KCl 1.0 M solutions.

The conductivity of the electrodes was characterized first by S-302 Signatone 4-point resistance probe connected to a Keithley 2410 nanovoltmeter. The samples were measured in five different spots, and the nanovoltmeter showed a resistance value for each. The average of the five resistances was obtained and the average conductivity was calculated for each thickness. SEM images were obtained with microscope Sigma 500 from Zeiss.

The DC resistance of the TGCs was characterized by chronoamperometry with the Bio-Logic SP 200. Fixed potentials between 1 and 200 mV were applied for 10 min, and the currents relative to each of the potentials were registered at $t = 10$ min. The DC resistance was calculated as the slope of the curve from the corresponding values of current and voltage. The electrochemical impedance spectroscopy (EIS) was utilized to characterize the device in a frequency range from 1 MHz to 1 mHz and applying AC perturbation of 5 mV.

For the Seebeck coefficient characterization, the TGCs were positioned between two Peltier elements, which were responsible for the temperature control through LabVIEW program. Two thermocouples were connected for temperature measurement on the electrode surface. The output voltage of the electrodes was monitored by a nanovoltmeter Keithley 2182 A. The stabilized temperature differences between the electrodes, typically after 5 min of ΔT applied. The slope (in mV K^{-1}) of the output voltage linearized with ΔT corresponds to the Seebeck coefficient. For the output power characterization, fixed ΔT was applied to the cell, and different load resistances (R_{LOAD}) were connected between the electrodes, allowing the extraction of an output current. With the output voltage and R_{LOAD} values, power output was calculated for the cells from the equation $P = V^2/R_{LOAD}$.

Supporting Information

Supporting Information is available from the Wiley Online Library or from the author.

Acknowledgements

This work has been financed by the EU Commission under the project Metatherm (Project 101058284), Swedish Research Council (Project 2024-04196, 2020-04210), ÅForsk Foundation, and the Advanced Functional Materials Center at Linköping University.

Conflict of Interest

The authors declare no conflict of interest.

Author Contributions

Pedro Santos Candiotto de Oliveira: formal analysis (lead); investigation (lead); methodology (lead); writing—original draft (lead). **Ujwala Ail**: investigation (supporting); methodology (supporting). **Zia Ullah Khan**: methodology (supporting); supervision (supporting). **Reverant Crispin**: conceptualization (equal); funding acquisition (equal); supervision (supporting); writing—review and editing (supporting). **Dan Zhao**: conceptualization (equal); funding acquisition (equal); supervision (lead); writing—original draft (supporting); writing—review and editing (lead).

Data Availability Statement

The data that support the findings of this study are available from the corresponding author upon reasonable request.

Keywords

activated carbon, electron transfer, energy harvesting, printed electrodes, redox electrolytes, sustainability, thermogalvanic cells

Received: December 17, 2024
Revised: February 3, 2025
Published online:

[1] M. Rahimi, A. P. Straub, F. Zhang, X. Zhu, M. Elimelech, C. A. Gorski, B. E. Logan, *Energy Environ. Sci.* **2018**, *11*, 276.
[2] D. Zhao, A. Würger, X. Crispin, *J. Energy Chem.* **2021**, *61*, 88.
[3] M. Massetti, F. Jiao, A. J. Ferguson, D. Zhao, K. Wijeratne, A. Würger, J. L. Blackburn, X. Crispin, S. Fabiano, *Chem. Rev.* **2021**, *121*, 12465.
[4] H. Zhou, H. Inoue, M. Ujita, T. Yamada, *Angew. Chem. Int. Ed.* **2023**, *62*, 202213449.
[5] H. Zhou, T. Yamada, N. Kimizuka, *J. Am. Chem. Soc.* **2016**, *138*, 10502.
[6] B. Yu, J. Duan, H. Cong, W. Xie, R. Liu, X. Zhuang, H. Wang, B. Qi, M. Xu, Z. L. Wang, J. Zhou, *Science* **2020**, *370*, 342.
[7] H. Inoue, H. Zhou, H. Ando, S. Nakagawa, T. Yamada, *Chem. Sci.* **2023**, *15*, 146.
[8] H. A. H. Alzahrani, M. A. Buckingham, F. Marken, L. Aldous, *Electrochem. Commun.* **2019**, *102*, 41.
[9] A. Sikdar, A. Majumdar, A. Gogoi, P. Dutta, M. Borah, S. Maiti, C. Gogoi, K. Anki Reddy, Y. Oh, U. Narayan Maiti, *J. Mater. Chem. A Mater.* **2021**, *9*, 7640.
[10] T. Schoetz, L. W. Gordon, S. Ivanov, A. Bund, D. Mandler, R. J. Messinger, *Electrochim. Acta* **2022**, *412*, 140072.
[11] M. A. Buckingham, F. Marken, L. Aldous, *Sustainable Energy Fuels* **2018**, *2*, 2717.
[12] M. Al Maimani, J. J. Black, L. Aldous, *Electrochem. Commun.* **2016**, *72*, 181.
[13] J. Wu, J. J. Black, L. Aldous, *Electrochim. Acta* **2017**, *225*, 482.
[14] K. Han, L. Xie, *Adv. Electron. Mater.* **2023**, *9*, 2300089.
[15] T. Kim, J. S. Lee, G. Lee, H. Yoon, J. Yoon, T. J. Kang, Y. H. Kim, *Nano Energy* **2017**, *31*, 160.
[16] K. Wijeratne, M. Vagin, R. Brooke, X. Crispin, *J. Mater. Chem. A Mater.* **2017**, *5*, 19619.
[17] M. S. Romano, N. Li, D. Antiohos, J. M. Razal, A. Nattestad, S. Beirne, S. Fang, Y. Chen, R. Jalili, G. G. Wallace, R. Baughman, J. Chen, *Adv. Mater.* **2013**, *25*, 6602.
[18] R. Hu, B. A. Cola, N. Haram, J. N. Barisci, S. Lee, S. Stoughton, G. Wallace, C. Too, M. Thomas, A. Gestos, M. E. Dela Cruz, J. P. Ferraris, A. A. Zakhidov, R. H. Baughman, *Nano Lett.* **2010**, *10*, 838.
[19] H. Im, T. Kim, H. Song, J. Choi, J. S. Park, R. Ovalle-Robles, H. D. Yang, K. D. Kihm, R. H. Baughman, H. H. Lee, T. J. Kang, Y. H. Kim, *Nat. Commun.* **2016**, *7*, 10600.
[20] L. Zhang, T. Kim, N. Li, T. J. Kang, J. Chen, J. M. Pringle, M. Zhang, A. H. Kazim, S. Fang, C. Haines, D. Al-Masri, B. A. Cola, J. M. Razal, J. Di, S. Beirne, D. R. MacFarlane, A. Gonzalez-Martin, S. Mathew,

© 2025 The Author(s). Advanced Energy and Sustainability Research published by Wiley-VCH GmbH

26999412, 0, Downloaded from https://advanced.onlinelibrary.wiley.com/doi/10.1002/aesr.202400428 by Linkoping Universitet, Wiley Online Library on [20/05/2025]. See the Terms and Conditions (https://onlinelibrary.wiley.com/terms-and-conditions) on Wiley Online Library for rules of use; OA articles are governed by the applicable Creative Commons License

Y. H. Kim, G. Wallace, R. H. Baughman, *Adv. Mater.* **2017**, *29*, 1605652.
[21] J. Park, T. Kim, *Nanomaterials* **2023**, *13*, 1488.
[22] X. Zhuang, H. Jin, B. Yu, H. Wang, Y. Luo, K. Liu, B. Hu, K. Xie, L. Huang, J. Duan, J. Zhou, *J. Mater. Chem. A Mater.* **2022**, *10*, 17544.
[23] P. Yang, K. Liu, Q. Chen, X. Mo, Y. Zhou, S. Li, G. Feng, J. Zhou, *Angew. Chem.* **2016**, *128*, 12229.
[24] C. Xu, Y. Sun, J. Zhang, W. Xu, H. Tian, *Adv. Energy Mater.* **2022**, *12*, 2201542.
[25] T. Ding, Y. Zhou, X. Q. Wang, C. Zhang, T. Li, Y. Cheng, W. Lu, J. He, G. W. Ho, *Adv. Energy Mater.* **2021**, *11*, 2102219.
[26] J. Duan, G. Feng, B. Yu, J. Li, M. Chen, P. Yang, J. Feng, K. Liu, J. Zhou, *Nat. Commun.* **2018**, *9*, 5146.
[27] A. Noori, M. F. El-Kady, M. S. Rahmanifar, R. B. Kaner, M. F. Mousavi, *Chem. Soc. Rev.* **2019**, *48*, 1272.
[28] M. C. G. Santos, *PhD Thesis,* Federal University of Minas Gerais **2020**.
[29] N. Elgrishi, K. J. Rountree, B. D. McCarthy, E. S. Rountree, T. T. Eisenhart, J. L. Dempsey, *J. Chem. Educ.* **2018**, *95*, 197.
[30] G. A. Tsirlina, *J. Solid State Electrochem.* **2017**, *21*, 1833.
[31] M. A. Buckingham, S. Hammoud, H. Li, C. J. Beale, J. T. Sengel, L. Aldous, *Sustainable Energy Fuels* **2020**, *4*, 3388.
[32] A. J. Bard, L. R. Faulkner, H. S. White, in *Electrochemical Methods: Fundamentals And Applications*, John Wiley & Sons, Hoboken, NJ **2022**.
[33] D. Pamuk, I. H. Taşdemir, A. Ece, E. Canel, E. Kiliç, *J. Braz. Chem. Soc.* **2013**, *24*, 1276.
[34] J. Lee. *PhD Thesis*, Curtin University **2014**.
[35] R. L. Lavall, P. S. C. de Oliveira, P. F. R. Ortega, J. P. C. Trigueiro, J. B. Gabriel, A. P. Heitmann, P. Chagas, C. C. Oliveira, L. C. A. Oliveira, *Chem. Eng. J.* **2023**, *455*, 140511.
[36] P. Yang, H. Fan, *Chem. Res. Chin. Univ.* **2020**, *36*, 420.
[37] T. K. M. Amaral, G. O. D, os Santos, P. S. C. De Oliveira, N. J. Pires, V. G. De Castro, G. G. Silva, A. M. L. Denadai, M. O. Alves, J. P. C. Trigueiro, R. L. Lavall, P. F. R. Ortega, *Chem. Eng. J.* **2020**, *388*, 124379.
[38] M. A. Buckingham, K. Laws, E. Cross, A. J. Surman, L. Aldous, *Green Chem.* **2021**, *23*, 8901.
[39] M. A. Buckingham, L. Aldous, *J. Electroanal. Chem.* **2020**, *872*, 114280.
[40] Y. Liu, M. Cui, W. Ling, L. Cheng, H. Lei, W. Li, Y. Huang, *Energy Environ. Sci.* **2022**, *15*, 3670.
[41] S. Wang, Y. Li, M. Yu, Q. Li, H. Li, Y. Wang, J. Zhang, K. Zhu, W. Liu, *Nat. Commun.* **2024**, *15*, 1172.

© 2025 The Author(s). Advanced Energy and Sustainability Research published by Wiley-VCH GmbH

26999412, 0, Downloaded from https://advanced.onlinelibrary.wiley.com/doi/10.1002/aesr.202400428 by Linkoping Universitet, Wiley Online Library on [20/05/2025]. See the Terms and Conditions (https://onlinelibrary.wiley.com/terms-and-conditions) on Wiley Online Library for rules of use; OA articles are governed by the applicable Creative Commons License